REFRACTION EFFECTS IN THE α AND ^{3}He SCATTERING ON ^{14}N NUCLEI AT ENERGIES ABOUT 50 MeV

N. Burtebayev[a], A. Duisebayev[a], B.A. Duisebayev[a]
M. Nassurlla[a], S.K. Sakhiev[a], B.M. Sadykov[a], S.B. Sakuta[b]
T.K. Zholdybayev[a], S. Kliczewski[c], R. Siudak[c]
M. Wolińska-Cichocka[d]

[a]Institute of Nuclear Physics, Ibragimova 1, 050032 Almaty, Kazakhstan
[b]National Research Center "Kurchatov Institute"
Kurchatov Sq. 1, 123182 Moscow, Russia
[c]The Henryk Niewodniczański Institute of Nuclear Physics
Polish Academy of Sciences
Radzikowskiego 152, 31-342 Kraków, Poland
[d]Heavy Ion Laboratory, University of Warsaw
Pasteura 5A, 02-093 Warszawa, Poland

(Received February 10, 2016; revised version received April 18, 2016)

The elastic and inelastic scattering of α-particles at 48.2 MeV and ^{3}He at 50 and 60 MeV energies on ^{14}N nuclei with excitation of the 3.95 MeV (1^+) and 7.03 MeV (2^+) states was studied. The analysis of angular distributions was performed using the coupled channels and distorted waves methods. A good description of the experimental data in the full angular range with potentials having volume integrals of the real part near 400–500 MeV fm^3 was obtained. The rainbow effects caused by refractive properties of the real nuclear potential were clearly seen in the measured angular distributions of the elastic scattering.

DOI:10.5506/APhysPolB.47.2017

1. Introduction

Analysis of scattering data within the optical model is the main source of information about potentials of the nucleus–nucleus interaction. It is well-known, however, that for complex projectiles with $A \geq 2$, such analysis is ambiguous. An especially complicated situation occurs at low energies ($E < 10$ MeV/nucleon). Numerous studies have shown that the ambiguity in the extracted parameters of the real part of the nuclear potential can be both continuous and discrete.

If the depth of the real part of the nuclear potential is large in comparison with the energy of the incident particle, which is a case at low E/nucleon < 10 MeV energies, then for sufficiently small impact parameters, due to the influence of nuclear attraction, the deflection angle of the scattered particle can exceed 180 degrees. In this case, a diffraction pattern is observed over the entire angular range of the angular distribution. However, at higher energies, the incident particle can be deflected on an angle not exceeding a certain limit. According to classical mechanics, the cross section at this point should become infinite. In quantum mechanics, however, the cross section is finite, but at not very strong absorption, a maximum should be observed followed by an exponential decrease at larger angles. This effect appears due to the refractive properties of the real part of the nuclear potential and is analogous to the phenomenon of the rainbow in optics. The magnitude and the angular dependence of the cross sections when the nuclear rainbow is observed are very sensitive to the real part of the nuclear potential as was first shown in papers [1, 2]. The analysis of such data using the optical model allows removing a discrete ambiguity in depth of the real part of the nuclear potential.

The nuclear rainbow features that are manifested in scattering of complex projectiles are discussed in a recent review [3]. It was shown that the following conditions must be met for a nuclear rainbow to be observed: the optical potential must be strongly attractive, absorption in the nuclear collisions must be weak and incident energy should be high enough. Observation of rainbow in the refraction scattering is very important as it can be used to probe the density dependence of the NN interaction and the nuclear equation of state in the folding model analysis.

Scattering of α-particles on ^{14}N nuclei was previously studied at energies from 20 to 30 MeV [4–6], 35 MeV [7], 40.5 MeV [8], 48.7 MeV [9], 54.1 MeV [9] and 104 MeV [10]. At energies less than 40 MeV [4–8], the diffraction structure in the elastic scattering is observed up to the far back angles. The analysis of [4], where measurements were taken in the full angular range, revealed discrete ambiguity in the choice of the optical potential. An equally good description of the experimental data was obtained with the different families of potentials having volume integrals of the real part from 200 to 1000 MeV fm^3. The character of the scattering varies strongly with increasing energy. It is here, however, that we have very little information. There are only two experimental works in which the studies were done at energies above 40 MeV. Thus, at energy of about 50 MeV [9], it has been shown that the diffractive structure is observed only in the forward hemisphere. Moreover, with increasing angle, it is damped and goes into a broad maximum at angle of about 90 degrees which is typical for nuclear rainbow scattering. The general character of the angular distribution does not change for higher

α-particle energy 104 MeV [10]. The only difference is that the whole structure is shifted toward smaller angles, and the rainbow bump is observed at an angle of about 40°.

Fewer data have been obtained for ^{3}He+^{14}N elastic scattering at energies above 20 MeV. Angular distributions have been previously measured at energies of 26.3 MeV [11] and 72 MeV [12] in the forward hemisphere. The nuclear rainbow effect occurs only at the energy of 72 MeV. In addition, we have earlier published results of measurements of elastic scattering at 50 and 60 MeV energies [13] with a preliminary analysis in the framework of the optical model.

Inelastic α-particle scattering with excitation of the ^{14}N nucleus was early studied only in two works [7, 8] at energies of 35–40 MeV in the angular range from 10° to 70°. Similar studies with ^{3}He were not conducted. Inelastic scattering on light nuclei is of interest from two points of view. Firstly, the structure of the low-lying states is sufficiently well-known what is important for the analysis and secondly, the level density is not high, permitting the measurement of differential cross sections even with not very good energy resolution.

A comparison of α-particles and ^{3}He inelastic scattering is also interesting. The angular dependence of the differential cross sections can be affected by the following factors. Firstly, the α-particle has a completely filled 1*s*-shell, and binding energy of the α-particle in light nuclei is approximately 10–15 MeV less than the binding energy of ^{3}He. We can, therefore, expect that the exchange processes $A(\alpha, A)\alpha$ and $A(^3\text{He}, A)^3\text{He}$ will give different contributions to the scattering. Secondly, in ^{3}He scattering, in contrast to α-particles, the contribution of a spin-orbit interaction can exist. And finally, for α-particles, the isoscalar excitations ($\Delta T = 0$) are possible only whereas for particles with $S \neq 0$, $T \neq 0$, the transitions with transfers of both spin and isospin are also available.

The aim of this work is to study the elastic and inelastic scattering of α-particles and ^{3}He on ^{14}N nuclei at energies of 50–60 MeV, *i.e.*, where the nuclear rainbow effects begin to manifest themselves clearly. These energies are sufficiently high to avoid the worst complications of compound nuclear effects.

2. Experimental procedure and results of measurements

The measurements were carried out with beams of α-particles and ^{3}He from the isochronous cyclotron U-150M of the Institute of Nuclear Physics (Almaty, Kazakhstan). The energy of α-particles was 48.2 MeV, while the ^{3}He energies were 50 and 60 MeV.

A gas target was used in the experiment. It is a cylindrical cell filled with natural nitrogen (99.61% of ^{14}N) to a pressure of about 1 atmosphere. The effective thickness of the target was in the range from 1 to 7 mg/cm^2, depending on the measurement angle. The uncertainty in the estimation of the thickness was not more than 3%. In more detail, the target design is described in [14].

Scattered particles were detected by a counter telescope consisting of two silicon detectors with thicknesses of 100 microns (ΔE) and 2 mm (E). The α-particles and ^{3}He were separated from other charged products of nuclear reactions by means of two-dimensional analysis technique (ΔE–E). The total energy resolution ranged from 400 to 500 keV, depending on the scattering angle. It was resulting mostly from the spread of the beam energy and the target thickness.

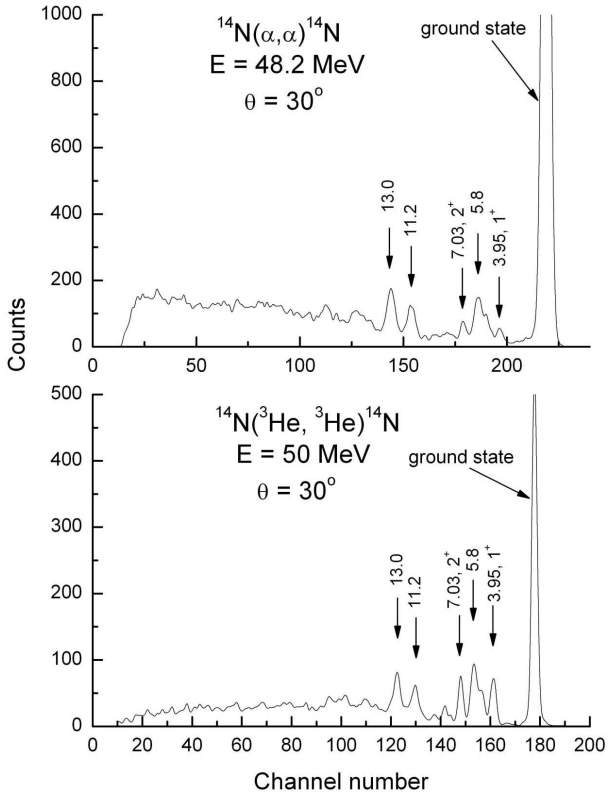

Fig. 1. The energy spectrum of the α-particles scattered at the 48.2 MeV energy on ^{14}N nuclei measured at the angle of 30° (upper panel). The energy spectrum of ^{3}He scattered at the 50 MeV energy on ^{14}N nuclei measured at the angle of 30° (bottom panel).

Typical spectra of the scattered particles are shown in Fig. 1. The elastic peak and well-separated transitions to states with excitation energies of 3.95 (1^+) and 7.03 MeV (2^+) are observed in the spectra of α-particles (upper panel). The peak at $E_x = 5.8$ MeV corresponds to two unresolved doublets in our experiment: 4.915 (0^-)–5.106 (2^-) and 5.691 (1^-)–5.834 (3^-). Besides the already mentioned transitions, the strong structures at $E_x = 11.2$ and 13.0 MeV appear at high excitation energies for all angles. These structures were also observed previously with better energy resolution for α-particles at 35 MeV [7]. No states of ^{14}N nuclei [15] with $T = 1$ which are known at excitation energy from 8 to 10 MeV together with the 2.31 MeV level ($J^\pi = 0^+$) were definitely observed to be excited.

The ^{3}He spectrum, as can be seen from Fig. 1 (lower panel), is very similar to the spectrum of α-particles. This indicates that the transitions to the levels with $T = 1$ in the scattering of ^{3}He and α-particles do not play a significant role.

Differential cross sections for elastic scattering have been measured in the range of angles from 10° to 170° in the laboratory system. Angular distributions, as can be seen from the figures shown in the next section, have a diffractive structure up to angles of 60°–70°. With increasing angle this structure decays and is replaced by a broad maximum with a further fall-off at larger angles without pronounced oscillations. In inelastic scattering with transitions to the states of 3.95 (1^+) and 7.03 MeV (2^+), measured up to angles of 100°–120°, the diffractive structure is less pronounced and at small angles, the cross sections oscillate out of phase with the elastic scattering.

The statistical uncertainties of the measured differential cross sections are less than 10%.

3. Analysis and discussion of the results

The measured angular distributions of the elastic and inelastic scattering were analysed by the coupled channels method using the FRESCO [16] program. Calculations of distortions in the input and output channels were carried out with a central potential without the spin-orbit interaction

$$U(r) = -V f_V(r) + i4a_W W_D \frac{\mathrm{d}f_W(r)}{\mathrm{d}r} + V_\mathrm{C}(r)\,. \tag{1}$$

The first two terms are responsible for the nuclear interaction potential with surface absorption. The radial dependence of $f_i(r)$ is described by the Woods–Saxon form factor with the reduced radius r_i and diffuseness $a_i (i = V, W)$

$$f_i(r) = \left[1 + \exp\left(\left(r - r_i A_\mathrm{t}^{1/3}\right) \Big/ a_i\right)\right]^{-1}\,. \tag{2}$$

V_C is a Coulomb potential of a uniformly charged sphere with radius R_C. For $r > R_C$, the Coulomb interaction between two nuclei is equal to

$$V_C = Z_p Z_t e^2 / r \,, \tag{3}$$

where Z_p, Z_t are projectile (p) and target (t) charges. $R_C = r_C A_t^{1/3}$ with $r_C = 1.3$ fm in all our calculations.

To find the optimal values of the parameters V, W_D, r_V, a_V, r_W, a_W, first the elastic scattering only was analysed using the optical model program SPI-GENOA [17]. The parameters were automatically searched for by fitting the calculated angular distributions to the experimental data by the least squares method with starting parameters proposed in [18]. For reducing the ambiguity of the search process, we have tried not to go far from the recommended values of the geometric parameters (r_V, a_V) of the real potential. For better agreement with the experimental data in the coupled channels calculations, the depth of the imaginary part (W_D) was only marginally reduced. The final parameters of the potentials are given in Table I.

TABLE I

Parameters of the potentials used in the coupled channels analysis.

a	E [MeV]	V [MeV]	r_V [fm]	a_V [fm]	W_D [MeV]	r_W [fm]	a_W [fm]	J_V [MeV fm^3]	J_W [MeV fm^3]
^{3}He	50	100.0	1.225	0.725	11.0	1.56	0.69	409.8	142.6
	60	102.0	1.225	0.725	13.0	1.56	0.69	418	168.5
^{4}He	48.2	145.0	1.200	0.890	6.88	1.61	0.80	509.4	84.7

As is seen from Table I, the volume integrals of the real part (J_V) normalized by the number of interacting pair of projectile and target nucleons ($1/A_p A_t$) are within 400–500 MeV fm^3. It is well-known that this integral is much better determined by data than the potential itself, as a relatively small variation of one of the potential parameters can be compensated by a small readjustment of the other (continuous ambiguity), while keeping the integral a constant. Thus, the volume integral plays as the representative of a given family of potentials. For interaction of ^{3}He and α-particles with $1p$-shell nuclei, it is believed that the most reasonable value of the volume integral is $J_V \sim 400$ MeV fm^3. This follows from the predictions of the microscopic theory (folding model) and phenomenological data analysis of the elastic scattering in the energy range from 10 to 200 MeV [9, 19, 20].

The coupling scheme used in the calculations, included elastic and inelastic scattering with transitions to the excited states of the ^{14}N nucleus (Fig. 2). The transitions between the ground and excited states were calcu-

lated in the framework of the rotational model with the form factor

$$V_\lambda(r) = \frac{\delta_\lambda}{\sqrt{4\pi}} \frac{\mathrm{d}U(r)}{\mathrm{d}r} \tag{4}$$

for quadrupole ($\lambda = 2$) transitions. Here, δ_λ is the deformation length ($\delta_\lambda = \beta_\lambda R$). The effects of the spin reorientation determined by the matrix element $\langle EJ^\pi|V_2|EJ^\pi\rangle$ were also included in the coupling scheme (Fig. 2). The deformation lengths extracted from the matching calculated inelastic cross sections in the full range of angular distributions are shown in Table II. As seen, the average value of δ_2 is 0.68 ± 0.32 fm.

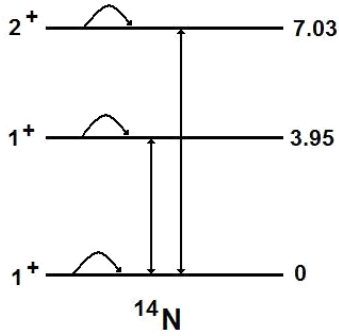

Fig. 2. The couplings scheme used in the coupled channels calculations of the elastic and inelastic scattering. The arcs show the spin reorientation of ground and excited states of ^{14}N.

TABLE II

Deformation lengths (δ_2) and interaction strengths (V_0), obtained from the analysis of inelastic scattering with FRESCO and DWUCK4 in the framework of macroscopic and microscopic models, respectively.

a	E [MeV]	e_x [MeV]	J^π	δ_2 [fm]	V_0 [MeV]
^{4}He	48.2	3.95	1^+	0.5	45
		7.03	2^+	0.5	45
^{3}He	50	3.95	1^+	0.7	45
	60	3.95	1^+	1.0	65

The analysis of inelastic scattering was performed not only in the macroscopic but also in the microscopic model in which the excitation is described as a single-particle transition between the orbits caused by the interaction of the incident particle and the nucleons of the target. In this case, the calculations were performed by the DWBA with zero-range interaction using the

program DWUCK4 [21]. The calculations were simplified by the fact that the structure of the excited states of the nucleus ^{14}N is well-known up to energy of 10 MeV. In particular, based on existing experimental data [22] and theoretical predictions of the shell model [23], the ground state has a configuration $(p_{1/2})^2_{j=1^+}$ over the ^{12}C core, and the excited 3.95 (1^+) and 7.03 MeV (2^+) levels have the hole structure $(p^{-1}_{3/2}p^{-1}_{1/2})_{j=1^+}$, $(p^{-1}_{3/2}p^{-1}_{1/2})_{j=2^+}$, respectively. Thus, these levels can be excited by promotion of a of $p_{3/2}$ nucleon from the ^{12}C core into the $p_{1/2}$ shell. For the $p_{3/2} \to p_{1/2}$ transition, the transferred angular momentum (l) can take the values $l = 0$ or 2, and transferred total angular momentum $j = 1$ or 2. Then, in the absence of spin-flip $(s = 0)$ and the parity change (π), according to the selection rule

$$j = l + s\,, \qquad \Delta\pi - (-1)^l\,, \tag{5}$$

l can only be 2.

The single-particle wave functions were calculated for the real Woods–Saxon potential with the reduced radius $r_0 = 1.25$ fm and diffuseness $a = 0.65$ fm. The depth of the potential was chosen for obtaining required binding energy of the nucleons.

For a rough estimate, the tensor component in the interaction, providing a $p_{3/2} \to p_{1/2}$ transition, can be neglected. Then, the effective interaction included only one central isoscalar part. Its radial dependence has the form of the Yukawa potential $V(r) = V_0 \exp(-\mu r)/(\mu r)$ with parameter $\mu = 0.7$ fm^{-1}. The interaction strength (V_0) was deduced from comparison the calculated cross sections with experimental data in the full angular range. The obtained values are shown in Table II. As seen, the mean value of V_0 is $V_0 = 55 \pm 10$.

The comparison of the calculations with the measured angular distributions of the elastic and inelastic scattering of α-particles and ^{3}He on ^{14}N with excitation of the 3.95 MeV (1^+) and 7.03 MeV (2^+) states is shown in Fig. 3 and Fig. 4. The solid curves are cross sections calculated by the coupled channels method with potentials from Table I and with the quadrupole deformation lengths δ_2 from Table II. The calculations reproduce well the observed diffraction structure of the elastic scattering in the forward hemisphere and a more gradual decline in the cross sections for medium and large angles (Fig. 3). The character of the angular distributions of inelastic scattering (Fig. 4) with weak diffraction structure is also described quite well both by the collective (solid curves) and the microscopic (dashed curves) models. It should be emphasized that the equally good description of the experimental data for α- particles and ^{3}He indicates that the exchange mechanism as well as the contribution of the spin-orbit interaction (for ^{3}He) does not play a significant role.

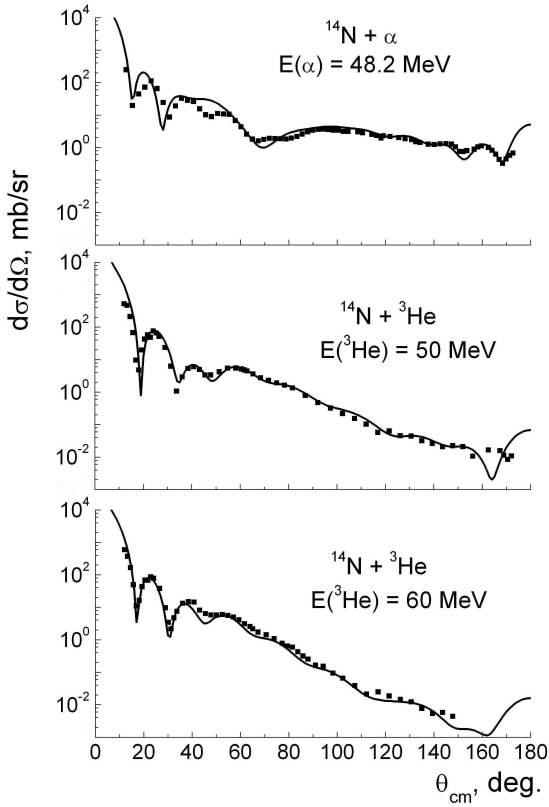

Fig. 3. The angular distributions of the elastic scattering of α-particles (E = 48.2 MeV) and ^{3}He at the 50 and 60 MeV energies on ^{14}N nuclei. The points are experimental cross sections. The curves are the coupled channels calculations.

The radial dependences for the real $V(r)$ and imaginary $W_D(r)$ parts of the found potentials (see Table I) are shown in Fig. 5 (a) and Fig. 5 (b), respectively. We note the following features. For α-particles, the depth of imaginary potential is less than the depth of the real potential both in the inner region of the nucleus and on the periphery outside the nuclear surface, while for ^{3}He at large distances values $V(r)$ and $W(r)$ are comparable $V(r) \approx W(r)$. The position of the nuclear surface, where the nuclear forces are coming into play, can be associated with the strong absorption radius ($R_{\rm sa}$). It is usually defined as the distance of the closest approach of two colliding nuclei in the Rutherford orbit for the partial waves $l_{\rm sa}$ with the transmission coefficient $T_l = 1 - |S_l|^2 = 0.5$ [24]

$$R_{\rm sa} = \frac{\eta}{k}\left\{1 + \left[1 + \left(\frac{l+1/2}{\eta}\right)^2\right]^{1/2}\right\}, \qquad (6)$$

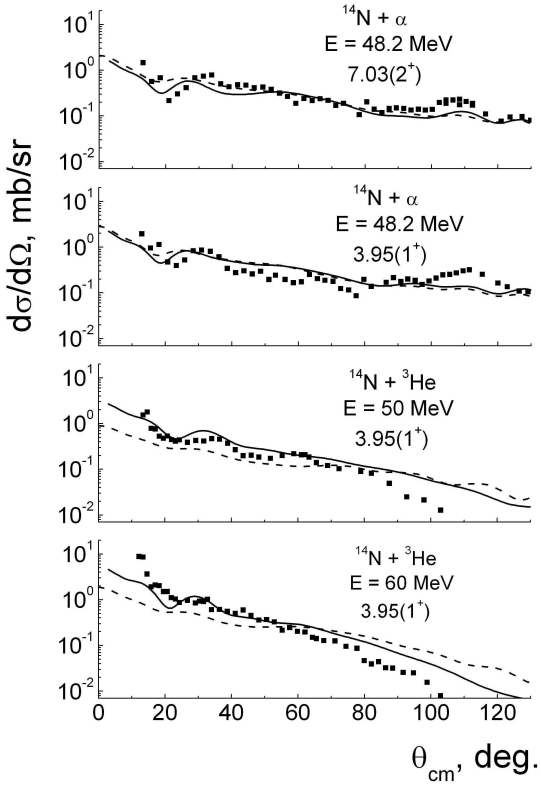

Fig. 4. The angular distributions of inelastic scattering of α-particles with 48.2 MeV energy and ^{3}He with 50 and 60 MeV energies on ^{14}N nuclei with excitation of states 3.95 MeV (1^+) and 7.03 MeV (2^+). The points are experimental cross sections. The solid curves are the coupled channels calculations with the collective model form factor. The dashed curves are the microscopic DWBA calculations.

where $k = \frac{\sqrt{2mE}}{\hbar}$, $\eta = \frac{Z_{\rm p}Z_{\rm t}e^2}{\hbar\nu}$ is the Sommerfeld parameter, $|S_l|$ is the module of the element of the elastic scattering S-matrix for the l partial wave. In this case, the value $R_{\rm sa}$ is within 4.8–5.0 fm.

More clearly, the role of absorption can be seen from Fig. 5 (c), where the function $w(r) = W(r)/V(r)$ is shown. It is sometimes called a reduced imaginary potential [25], since it can be interpreted as the flux removal from the elastic channel $W(r)$, weighted by the distribution of the inverse matter density which is approximately characterized by $V(r)$. It can be seen that the maximum of the function occurs in the region near the strong absorption radius $R_{\rm sa}$. The values of the modulus of the scattering matrix elements $|S_l|$ for the potentials from Table I are shown in Fig. 6. The curves from Fig. 6 show the absorption profiles of the particles scattered by the

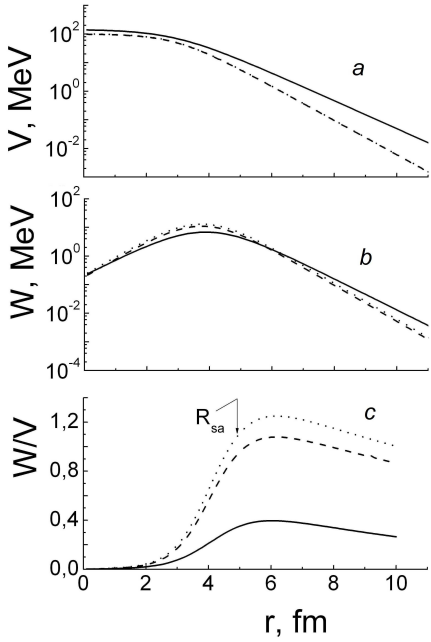

Fig. 5. The radial dependences of the real ($V(r)$) (a), imaginary ($W_D(r)$) (b) parts of potentials from Table I and their ratio W_D/V (c). The solid curves refer to α-particles. The dashed and dotted curves refer to the ^{3}He projectiles with the 50 MeV and 60 MeV energy, respectively.

potential. For the partial waves, $l > 15$ absorption practically does not appear ($T_l \ll 1$), but also for small waves ($l < 10$), associated with the passage of particles inside the nucleus, transparency is still quite large ($T_l \sim$ 0.9–0.95). According to study of ^{3}He elastic scattering on ^{13}C nuclei at energies of 50 and 60 MeV [26], the sensitivity to the real part of the nuclear potential is maximal in this area ($r < 5$ fm). Consequently, the differential cross sections of the scattering at large angles should be determined mainly by the refractive properties of the real part of the potential at small distances.

The qualitative picture of the elastic scattering is most easily understood in terms of semi-classical trajectories. This approach is justified, since the number of partial waves contributing to the scattering, as shown in Fig. 6, is sufficiently large.

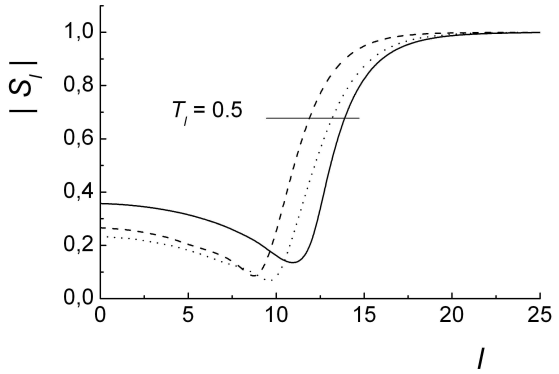

Fig. 6. The modulus of the S_l matrix elements for potentials from Table I. The solid curves refer to α-particles. The dashed and dotted curves refer to ^{3}He with 50 MeV and 60 MeV energy, respectively.

Much of the interpretation becomes especially transparent when couched in the semiclassical language. So, the differential cross section at a given angle is determined by the contribution of the trajectories corresponding to scattering on the near and far edges of the nucleus with amplitudes $f_{\rm N}(\theta)$ and $f_{\rm F}(\theta)$, respectively [27]. In the scattering at the near edge, the Coulomb interaction dominates, while at the far edge, the nuclear interaction prevails. Then, the total scattering amplitude has the form

$$f(\theta) = f_{\rm N}(\theta) + f_{\rm F}(\theta)\,. \tag{7}$$

The differential cross sections, corresponding to these components, were calculated using potentials from Table I by the FRESCO program. They are compared with experimental angular distributions of the elastic scattering in Fig. 7. As can be seen from this figure, $f_{\rm F}(\theta) < f_{\rm N}(\theta)$ at small angles, but the amplitude of the near components decreases with angle much faster, so that at a certain angle, amplitudes intersect ($f_{\rm F}(\theta) = f_{\rm N}(\theta)$). On the large angles, scattering at the far edge of the nucleus dominates. The interference pattern, which is especially pronounced near the point of intersection of two components, is corresponding to the double-slit Fraunhofer diffraction in optics with the maxima which are spaced by $\Delta\theta = \pi/l_{\rm sa}$ [25]. And this is observed in the experimental angular distributions ($\Delta\theta \approx 15^\circ$). The far component reproduces the unstructured nature of the angular distributions at medium angles with a distinct broad maximum and an exponential falloff at the larger angles. It should be noted that for angles 120° to 140° $f_{\rm F}(\theta)$ and $f_{\rm N}(\theta)$ the amplitudes converge again, and a diffractive structure reappears. However, it is much less pronounced then for small angles.

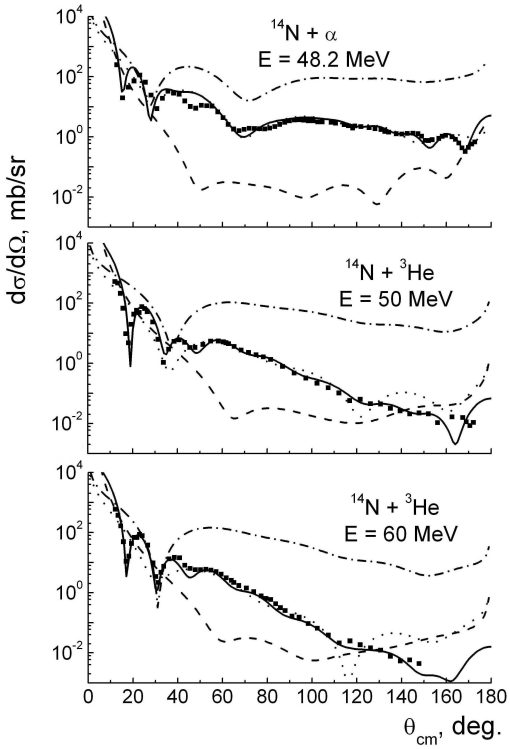

Fig. 7. Comparison of calculated and experimental cross sections for the elastic scattering of α-particles with 48.2 MeV energy and ^{3}He with 50 and 60 MeV energies. The points are experimental cross sections. The dotted and dashed curves are calculations for the near-side and far-side components, respectively. The solid curves are calculated total cross sections. The dot-dashed curves are calculations for the far components with $W = 0$.

A broad maximum and monotonic decrease of the cross sections at the larger angles, observed in the angular distributions, are associated with the presence of the limit angle in the deflection function, and caused by the refractive properties of the nuclear potential, or rather its real part. According to classical mechanics, at this angle, the cross section must be infinite, and for high angles, in the shadow area, must vanish. By analogy with classical optics, this angle (θ_{R}) is called a nuclear rainbow angle. The presence of the absorption can significantly distort the effect of the nuclear rainbow in the angular distributions. To make the situation more transparent, the cross sections were calculated for the far component with imaginary part equal to zero ($W = 0$) for the potentials from Table I. Calculations, as can be seen from Fig. 7, show that the maximum and subsequent slope, observed in the angular distributions, are really connected with the refractive properties of

the nuclear potential, and the absorption leads only to an overall reduction of cross sections. The structure observed at $\theta < \theta_R$ in cross sections for the far components, especially pronounced at $W = 0$, is associated with the interference of two trajectories with $l_<$ and $l_>$ for the same negative angle of the deflection function f_F. Such structure is described by the Airy function [28] with alternating maxima and minima. These oscillations have a width $\Delta\theta = \pi/(l_> - l_<)$, significantly greater than the corresponding value for the oscillations resulting from the interference of $f_F(\theta)$ and $f_N(\theta)$. It should be noted that for ^{3}He scattering at energies of 50 and 60 MeV, only one Airy minimum (at the angles of 35° and 30°, respectively) is observed, while for the α-particles two minima are seen, one at the 70° angle (primary rainbow) and the other at the 28° angle (secondary rainbow).

It is known [29] that with increasing energy of the incident particle, the rainbow angles are shifted according to the law $\theta \sim 1/E$. This is demonstrated in Fig. 8, which shows dependence of the first Airy minimum position on the ^{3}He energy.

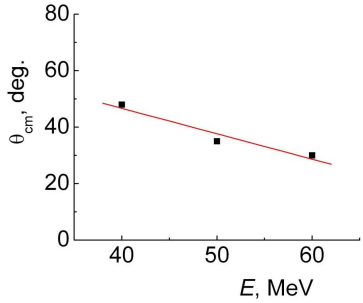

Fig. 8. The position of the Airy minimum as the function of the ^{3}He energy. The point for 40 MeV is taken from [12].

Thus, in the elastic scattering of α-particles and ^{3}He on ^{14}N nuclei at energies around 50 MeV, the effects of rainbow, caused by the refractive properties of the nuclear potential, are clearly observed.

4. Conclusions

The elastic and inelastic scattering of α-particles with 48.2 MeV energy and ^{3}He with 50 and 60 MeV energies (with excitation of 3.95 MeV (1^+) and 7.03 MeV (2^+) states) on ^{14}N nuclei was studied. The measured angular distributions were analysed by the coupled channels method. Transitions to excited states were calculated in the framework of the collective model taking into account the spin reorientation. A good description of the experimental data was obtained without the inclusion of exchange mechanisms and the spin-orbit interaction. This indicates that they do not play an important

role in the scattering α-particles and ^{3}He at energies about 50 MeV. The microscopic model with a Yukawa effective interaction also describes the inelastic scattering, demonstrating that there is little model dependence for our conclusions.

The volume integrals of the found real potentials are within the 400–500 MeV fm^3 interval, which is consistent with the predictions of the microscopic theory and with the results of the global analysis of the elastic scattering of α-particles and ^{3}He in the 10–200 MeV energy range. The radial dependence of ratio of the imaginary and real potentials $W(r)/V(r)$ is characterized by a maximum near the strong absorption radius ($R_{\rm sa}$), and the potentials themselves indicate a rather high transparency for small partial waves in the region of maximal sensitivity to the real part at $r < R_{\rm sa}$.

The effects of the nuclear rainbow are clearly observed in the measured angular distributions of the elastic scattering. This is indicated by the following.

1. The presence of the Fraunhofer oscillations in the forward hemisphere. The oscillations are especially significant at the angles where the amplitudes for the scattering on the near and far edges of the nucleus are comparable.
2. The presence in the angular distributions of a broad maximum and subsequent monotonic falloff in the cross sections at the larger angles. This is associated with the existence of the limit angle in the deflection function of the particle scattered in the attractive nuclear field.
3. Reproduction of the observed structure in the far component due to refractive properties of the nuclear potential, including the calculations without imaginary part. This indicates that the observed decrease of the cross sections on the larger angles is due the refractive properties of the nuclear potential and not by the absorption.
4. The periods of the oscillation structures observed in the angular distributions, both in the total cross sections and in the far component are consistent with the predictions of the semiclassical theory of the rainbow scattering.
5. The energy dependence of the Airy minimum position for the far component is consistent with the prediction of the semiclassical model.

This work was supported in part by a grant of MES RK, Project "Experimental and theoretical investigation of elastic and quasi-elastic processes of interaction of ^{3}He and d ions with the p- and sd-shell nuclei". We thank Prof. R.J. Peterson (University of Colorado) for numerous discussions of the results and valuable comments.

REFERENCES

[1] D.A. Goldberg, S.M. Smith, *Phys. Rev. Lett.* **29**, 500 (1972).

[2] D.A. Goldberg, S.M. Smith, G.E. Burdzik, *Phys. Rev. C* **10**, 1362 (1974).

[3] D.T. Khoa, W. von Oertzen, H.G. Bohlen, S. Ohkudo, *J. Phys. G: Nucl. Part. Phys.* **34**, R111 (2007).

[4] J.B.A. England, J. Aguilar, H.M. Gupta, *Nucl. Phys. A* **284**, 29 (1977).

[5] M. Oeschler *et al.*, *Phys. Rev. Lett.* **28**, 694 (1972).

[6] B.I. Kuznetsov, P.E. Ovsyannikova, I.P. Tschernov, *Yad. Fiz.* **15**, 673 (1972) [*Sov. J. Nucl. Phys.* **15**, 377 (1972)].

[7] R.J. Peterson, J.J. Hamill, *Z. Phys. A* **305**, 275 (1982).

[8] B.G. Harvey *et al.*, *Phys. Rev.* **146**, 712 (1966).

[9] H. Abele *et al.*, *Z. Phys. A* **326**, 373 (1987).

[10] G. Hauser *et al.*, *Nucl. Phys. A* **128**, 81 (1969).

[11] A.M. Mukhamedzhanov *et al.*, *Phys. Rev. C* **67**, 65804 (2003).

[12] A.S. Demyanova *et al.*, *Phys. Scr.* **T32**, 89 (1990).

[13] V.V. Adodin, N.T. Burtebayev, A.D. Duisebayev, *Yad. Fiz.* **55**, 577 (1992).

[14] A.D. Duisebayev *et al.*, *Izv. AN Kaz. SSR, Ser. Fiz.-Mat.* **4**, 73 (1984).

[15] F. Ajenberg-Selove, *Nucl. Phys. A* **523**, 1 (1991).

[16] I.J. Thompson, *Comput. Phys. Rep.* **7**, 167 (1988) available at: `http://www.fresco.org.uk/`

[17] F. Perey, SPI-GENOA, An Optical Model Search Code (unpublished).

[18] G.R. Satchler, W.G. Love, *Phys. Rep.* **55**, 183 (1979).

[19] R. Görgen *et al.*, *Nucl. Phys. A* **320**, 296 (1979).

[20] H.-J. Trost, P. Lezoch, U. Strohbusch, *Nucl. Phys. A* **462**, 333 (1987).

[21] P.D. Kunz, computer program DWUCK4, Zero Range Distorted Wave Born Approximation (unpublished), available at: `http://spot.colorado.edu/~kunz/DWBA.html`

[22] E.K. Warburton, W.T. Pinkston, *Phys. Rev.* **118**, 733 (1960).

[23] W.W. True, *Phys. Rev.* **130**, 1530 (1963).

[24] G. Madurga, A. Jadraqua, M. Lozano, *Phys. Rev. C* **23**, 1536 (1981).

[25] M.E. Brandan, G.R. Satchler, *Phys. Rep.* **285**, 143 (1997).

[26] N.T. Burtebayev, A.D. Duisebayev, B.A. Duisebayev, S.B. Sakuta, *Yad. Fiz.* **63**, 625 (2000).

[27] M.S. Hussein, K.W. McVoy, *Prog. Part. Nucl. Phys.* **12**, 103 (1984).

[28] L.D. Landau, E.M. Lifschitz, Kvantovaya mechanika, Vol. 3, Nauka, Moskva, 1973 (in Russian).

[29] J. Knoll, R. Schaeffer, *Ann. Phys.* **97**, 307 (1976).